Molecular Therapy
Nucleic Acids
Original Article

Poly-Target Selection Identifies Broad-Spectrum RNA Aptamers

Khalid K. Alam,[1,2,5] Jonathan L. Chang,[2,3] Margaret J. Lange,[2,3] Phuong D.M. Nguyen,[1,2] Andrew W. Sawyer,[1,2] and Donald H. Burke[1,2,3,4]

[1]Department of Biochemistry, University of Missouri, Columbia, MO, USA; [2]Bond Life Sciences Center, University of Missouri, Columbia, MO, USA; [3]Department of Molecular Microbiology and Immunology, University of Missouri, Columbia, MO, USA; [4]Department of Biological Engineering, University of Missouri, Columbia, MO, USA

Aptamer selections often yield distinct subpopulations, each with unique phenotypes that can be leveraged for specialized applications. Although most selections aim to attain ever higher specificity, we sought to identify aptamers that recognize increasingly divergent primate lentiviral reverse transcriptases (RTs). We hypothesized that aptamer subpopulations in libraries pre-enriched against a single RT may exhibit broad-spectrum binding and inhibition, and we devised a multiplexed poly-target selection to elicit those phenotypes against a panel of primate lentiviral RTs. High-throughput sequencing and coenrichment/codepletion analysis of parallel and duplicate selection trajectories rapidly narrowed the list of candidate aptamers by orders of magnitude and identified dozens of priority candidates for further screening. Biochemical characterization validated a novel aptamer motif and several rare and unobserved variants of previously known motifs that inhibited recombinant RTs to varying degrees. These broad-spectrum aptamers also suppressed replication of viral constructs carrying phylogenetically diverse RTs. The poly-target selection and coenrichment/codepletion approach described herein is a generalizable strategy for identifying cross-reactivity among related targets from combinatorial libraries.

INTRODUCTION

Aptamers are single-stranded nucleic acids that bind with high affinity to defined molecular targets, and they can be generated through an iterative *in vitro* selection process known as systematic evolution of ligands by exponential enrichment (SELEX).[1–3] Although the aptamer field has traditionally sought to maximize selectivity and molecular discrimination among related molecular targets, aptamers with broad target recognition can be especially useful for recognizing entire classes of chemically related metabolites or evolutionarily related protein families. In a therapeutic context, broad-spectrum aptamers that bind to highly conserved residues of a rapidly evolving protein (e.g., viral proteins) would present a higher genetic barrier to the emergence of drug resistance than would highly specific aptamers. Similarly, aptamers that bind to entire families of biomolecular or chemical targets would be useful in diagnostics (e.g., for measurement of total glucocorticoids) and as research tools to contrast against highly specific aptamers. Within synthetic biology, where aptamers are often engineered into riboswitches to regulate gene expression, broad-spectrum aptamers that are responsive to an entire class of molecules would increase our ability to fine-tune regulation strategies. In the present work, we explore this theme by seeking aptamers that recognize increasingly divergent representatives of the primate lentiviral family of reverse transcriptases (RTs).

RNA aptamers selected against HIV-1 RT are able to bind RT and inhibit its enzymatic activities, and they overwhelmingly form pseudoknot structures.[4–7] These pseudoknot RNA aptamers show robust *in vitro* inhibition of the RT they were selected to bind,[8] and they suppress viral replication and infectivity in cell culture.[9–13] Structural and biophysical investigations suggest that these pseudoknot RNA aptamers bind the closed conformation of RT in a positively charged groove, 50–60 Å in length, that spans the polymerase and RNase H domains.[14,15] This same groove can accommodate 16–19 bp of nucleic acid and naturally binds a duplex of viral RNA and host $tRNA_{Lys}$ primer. An observation from our lab is that a common polymorphism in this groove, near the polymerase active site (K277 in the p66 subunit), confers resistance to the family 1 pseudoknot (F1Pk) subset of RNA aptamers, but not the family 2 pseudoknot (F2Pk) subset,[16] thereby preventing broad-spectrum inhibition. In contrast, single-stranded DNA aptamers selected against RT[17] demonstrate broad-spectrum inhibition *in vitro*,[18–21] but their use in cell culture assays of viral replication or *in vivo* is complicated by the requirement to produce or deliver single-stranded DNA in the relevant cells.

High-throughput sequencing (HTS) of anti-RT RNA aptamer libraries recently revealed several additional motifs capable of RT binding and inhibition, including the (6/5) asymmetric loop ((6/5)AL)[7] and the UCAA bulge.[22] These non-pseudoknot motifs were difficult to detect with low-throughput sequencing, as their low sampling frequencies were eclipsed by the abundance of aptamers that carried

Received 30 July 2018; accepted 19 October 2018;
https://doi.org/10.1016/j.omtn.2018.10.010.

[5]Present address: Department of Chemical and Biological Engineering, Northwestern University, Evanston, IL, USA

Correspondence: Donald H. Burke, Bond Life Sciences Center, University of Missouri, 471H Bond Life Sciences Center, Columbia, MO 65211, USA.
E-mail: burkedh@missouri.edu

F1Pk or F2Pk motifs (>93% in one library).[7] Although these novel motifs were neither selected nor initially characterized specifically for their broad-spectrum inhibition, recent work, done in conjunction with the work described here, demonstrated that these non-pseudoknot motifs were capable of broad-spectrum suppression of viral replication when actively encapsidated into nascent virions.[13] These results indicate that even within a highly evolved library, there remains an important untapped phenotypic diversity that is difficult to capture by conventional selection strategies. The central goal of the present work is to demonstrate a general method that can be used to find aptamer subsets with broad-spectrum target recognition for any family of proteins. The additional functional diversity present in the RT-binding libraries suggested that new genotypes and phenotypes were potentially accessible under different selection conditions and made them ideal for demonstrating the approach.

Herein we describe a poly-target selection method to enrich for RNA aptamer subpopulations with broad-spectrum binding and inhibition of diverse primate lentiviral RTs. Rather than performing a *de novo* selection from a random-sequence library, we used two well-characterized libraries that had been pre-enriched for binding RT from a specific HIV-1 strain. Negative selections against nitrocellulose were performed to remove RT-independent binders, followed by three rounds of positive selection against a panel of seven diverse primate lentiviral RTs, in parallel. Each selection trajectory was performed in duplicate, and HTS of the starting, negative, and final libraries enabled an informatics approach to rapidly identify candidate aptamers through coenrichment/codepletion analysis of the various selection trajectories. Structural and biochemical characterization of candidates identified several rare or previously unobserved variants of known motifs and one previously unknown motif capable of varying degrees of broad-spectrum inhibition of RT polymerase activity. Furthermore, these broad-spectrum aptamers inhibited RTs from subtype C, the most prevalent subtype of HIV-1, and other clades that were not included in the selection panel and suppressed viral replication of constructs containing diverse RTs. We believe the poly-target selection method is broadly applicable to any aptamer or combinatorial selection approach that seeks to identify cross-reactivity for applications in therapeutics, diagnostics, and synthetic biology.

RESULTS

Poly-Target Selection Panel

Two distinct, pre-enriched aptamer libraries with randomized regions of either 70 or 80 nt (70N and 80N, respectively) were used to initiate poly-target selection. These libraries were originally selected *in vitro* against recombinant RT from a group M, subtype B strain of HIV-1 (BH10).[6] In these original selections, partitioning for protein-bound RNA was accomplished through 11 rounds of nitrocellulose filtration and 3 rounds of native gel shifts, for a total of 14 rounds. The vast majority of RNA aptamers in these populations form pseudoknot structures, with much lower frequencies of other, previously undetected motifs, such as the (6/5)AL[7] and UCAA bulge.[22] All of these motifs bind with low nanomolar affinity and inhibit RT by competing with primer template for access to the enzyme. The presence of additional, low-abundance, high-affinity aptamers suggested that significant diversity exists within these round 14 libraries. The focus of the present work was to exploit untapped diversity within these pre-enriched libraries by identifying low-abundance structural motifs that may offer broad-spectrum binding and inhibition of RTs.

To elicit broad-spectrum phenotypes from the pre-enriched libraries, we assembled a panel of phylogenetically diverse primate lentiviral RTs (Figure 1).[16] The panel of targets included RTs from multiple strains of the major group (group M) of HIV-1, which is responsible for the global HIV pandemic and is further divided into subtypes and circulating recombinant forms (CRFs) that contain genomic segments from two or more subtypes. HXB2 is a group M, subtype B strain closely related to the original selection target (98.9% by amino acid identity), and it is often used as a reference strain for sequence comparisons. We therefore included RT from strain HXB2 in the panel as a "continuity control." Also included was an R277K single-point mutant of HXB2, a natural polymorphism that confers resistance to inhibition by F1Pk aptamers *in vitro*[16] and in cell culture,[13] to enrich for aptamers that bind despite this escape mutation (henceforth referred to as R277K). RT from strain 94CY was included as a representative of subtype A HIV-1, along with RT from 93TH, which groups phylogenetically within CRF01_AE, a CRF that carries genomic segments corresponding to subtypes A and E.

The selection panel also included RTs from HIV-1 strains from outside group M and from simian immunodeficiency virus (SIV_{cpz}*Pts*). Although these additional strains are of less epidemiological relevance, they help capture the broader genetic diversity of primate lentiviruses (Figure S1). The outlier group of HIV-1 (group O) is phylogenetically distinct from group M and was therefore represented in the selection panel by an RT from the group O strain MVP. Because HIV-1 arose from zoonotic transmission of SIV_{cpz} from chimpanzees,[23] we included an RT from the TAN1B strain of SIV_{cpz}. Finally, we included RT from the EHO strain of HIV-2, which is only distantly related to HIV-1, to further broaden the scope of the poly-target selection. Selecting independently against each of these RTs presents a gradient of selection pressures on the pre-enriched library to search the sequence space for ligands that are capable of making molecular contacts with conserved features of primate lentiviral RTs. The unabbreviated names of the strains, their reference sequences, and amino acid changes relative to the database reference sequences are provided in Table S1.

Poly-Target Selection, HTS, and Bioinformatics

A schematic for the poly-target selection strategy is shown in Figure 1. Pre-enriched round 14 libraries (70N and 80N) were transcribed and partially depleted for nitrocellulose-binding species. Libraries were then separated into replication populations (A and B) and further split into independent populations for each of the seven RT targets. For each round of poly-target selections, 200 pmol ($\sim 1.2 \times 10^{14}$ molecules) of transcribed RNA for a given trajectory was independently

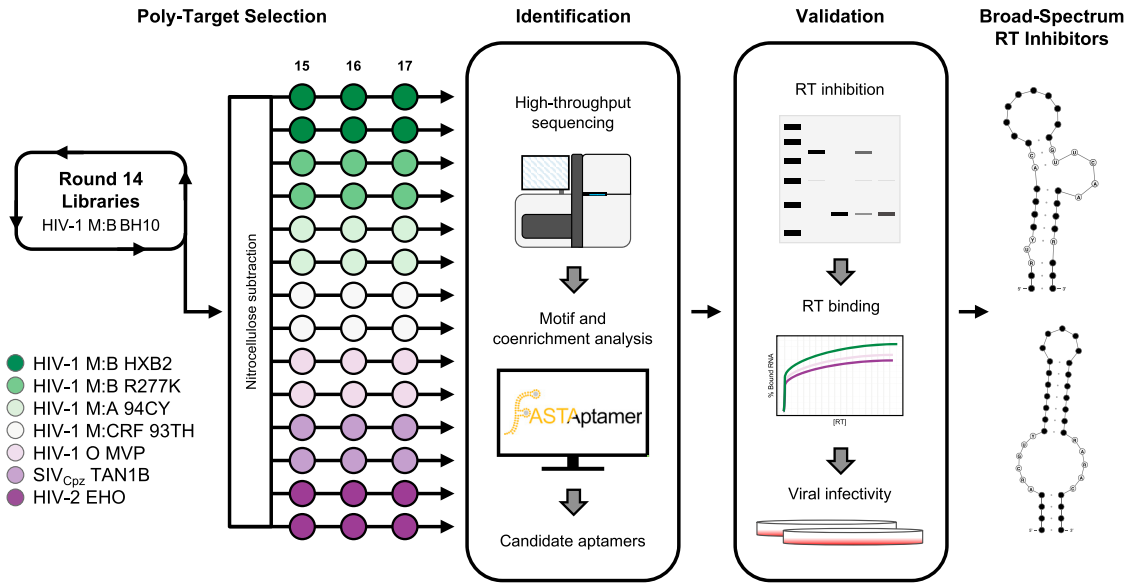

Figure 1. A Poly-target Selection Strategy to Identify Broad-Spectrum RT Inhibitors

In the poly-target selection approach, a pre-enriched aptamer library is subjected to additional rounds of systematic evolution of ligands by exponential enrichment (SELEX) against a panel of related targets along separate trajectories. In this work, 70N and 80N libraries that had been pre-enriched through 14 rounds of binding to an RT from HIV-1 M:B (BH10)[6] were first subjected to a negative selection (nitrocellulose subtraction) prior to three additional rounds of independent selections, in duplicate, against a panel of phylogenetically distinct RTs from various strains of HIV-1, HIV-2, and SIV. Following the poly-target selection, high-throughput sequencing and coenrichment analysis were used to identify candidate broad-spectrum aptamers for downstream biochemical and biological validation.

incubated with a single RT from the selection panel. Bound RNA:RT complexes were captured on nitrocellulose filters, and the recovered RNA was reverse-transcribed into cDNA and then PCR-amplified for additional rounds of selection or for HTS. Each selection trajectory was performed for a total of three rounds, after which the starting round 14 libraries, the nitrocellulose-binding populations, and the round 17 libraries were submitted for HTS.

HTS of the libraries generated more than 184 million raw reads. Demultiplexing, trimming, and quality filtering (Figure S2) of sequences left more than 52 million high-quality reads for the 70N library and 54 million for the 80N library. Each selection trajectory contained an average of 3 million total reads and 35,000 to >100,000 unique sequences (Table S2). The average number of reads per unique sequence increased for all populations, indicating enrichment and convergence on sequence space within each library, with the exception of 70N TAN1B (A), which was the only population with fewer than 1 million total reads (Figure S3). Aptamer populations were further processed by the FASTAptamer[24] toolkit to determine sequence frequencies, compare populations, and calculate enrichment of each unique sequence relative to the starting round 14 library. Sequences were clustered with FASTAptamer using Levenshtein edit distance, a string similarity metric that calculates the minimum number of insertions, deletions, and substitutions necessary to transform one sequence into another. Sequences within a small edit distance from each other likely diverged from a parent sequence in an earlier population, and grouping them into a single cluster simplifies analysis. On the basis of previous observations that sequences in these populations typically diverge by less than 10% from their parent sequences,[7] we defined clusters as having a maximum edit distance of 7 for the 70N library and 8 for the 80N library.

To determine the degree to which replicate selections against the same target experienced similar evolutionary paths, normalized sequence frequencies from the A and B trajectories for each target were compared using FASTAptamer-Compare.[24] For both the 70N and 80N round 14 libraries, we observed a tight $y = x$ relationship between replicates (Figures S4A and S5A), suggesting highly similar input diversity for each pair of replicate trajectories for a given target. In contrast, comparing sequence frequencies between replicate trajectories after three rounds showed a multimodal distribution for many populations, wherein different subsets of sequences either enrich, remain neutral, or deplete (Figures S4B–S4H and S5B–S5H). These minor variations between replicate trajectories likely reflect stochastic variations in sample handling[25] and highlight the potential value in providing multiple, independent evolutionary opportunities for a given sequence to enrich or deplete. As expected, distributions were widened more dramatically when comparing different selection rounds or selections against different targets (Figures S6 and S7).

Coenrichment Analysis Identifies Candidate Broad-Spectrum Aptamers

Sequences from the poly-target selection that enriched in more than one selection trajectory were expected to be the most promising candidates as broad-spectrum aptamers. As a first step toward coenrichment analysis, we identified sequences within each post-selection

population that met a given enrichment threshold, which we defined as a 2-fold or greater increase in reads per million (RPM) relative to the starting round 14 population (Figure S8A). To mitigate the potential impact of low-abundance sampling artifacts, we confined this analysis to sequences with an aggregate RPM $\geq$ 10 when summed across the populations being compared (e.g., round 14 RPM + round 17 RPM). We also included sequences that were below the detection limit in round 14 libraries but later increased in relative abundance and were sampled with $\geq$10 RPM in round 17, although their absence in round 14 precluded calculating an enrichment ratio. On average, each trajectory had approximately 1,800 sequences that met these enrichment criteria (Table S3). Depleting sequences were similarly flagged by identifying sequences with aggregate RPMs of $\geq$10 that either decreased by at least 2-fold (0.5-fold enrichment) in each trajectory or that were present in round 14 at $\geq$10 RPM and below the detection limit in round 17. Each trajectory had approximately 2,600 sequences that met these depletion criteria (Table S3). In nearly all trajectories, the number of sequences that depleted throughout the course of the selections exceeded the number that enriched.

We reasoned that broad-spectrum aptamers should enrich along multiple selection trajectories, while specialist aptamers should deplete in most or all trajectories. Therefore, we next identified the sets of sequences that experienced coenrichment or codepletion in two or more trajectories (Figure S8B). These were pooled according to starting library and replicate, irrespective of which individual trajectories provided the basis for identifying them as coenriching or codepleting. Each starting library (70N and 80N) and each replicate within them (A and B) were analyzed independently, thereby generating four unique sets of coenriched sequences (average of 3,200 per set) and four sets of codepleted sequences (average of 3,500 per set) (Table S4). Sequences demonstrating coenrichment or codepletion in the negative nitrocellulose selections were eliminated from analysis, reducing each library replicate to an average of 2,500 coenriched and 1,800 codepleted sequences. Dataset complexity was further reduced by reclustering each set of coenriched or codepleted sequences into sequence families. To facilitate comparison across trajectories, the identified sequences were mapped to their cluster identity from round 14 (Figure S9). Clustering and mapping in this manner allowed us to readily discern highly enriched clusters that arose in either or both replicate trajectories.

As individual clusters can contain numerous sequence variants, individual sequences within those clusters can sample advantageous or deleterious mutations. To focus on clusters where the majority of sequences exhibited coenrichment with minimal codepletion, we coupled the output from the coenrichment and codepletion analysis (Figure S10). Fourteen clusters from the 70N libraries and 19 clusters from the 80N libraries were chosen for further characterization on the basis of this analysis (33 total clusters). Two clusters that heavily depleted in the 70N trajectory (70N 2 and 70N 3) were also included to test whether codepletion is predictive of low fitness. For each cluster, the most abundant corresponding sequence in round 14 was chosen to represent the entire cluster in biochemical characterization. Candidate aptamers are named by their library of origin and their cluster identity in the pre-enriched round 14 libraries (e.g., aptamer 70N 89 is the 89th most abundant cluster-defining sequence in the 70N round 14 library). Sequences that were not sampled in the round 14 libraries were named according to the cluster identity generated in the coenrichment analysis. A heatmap of genotypic frequencies for each selected candidate aptamer in each trajectory is shown in Figure 2A, with more detailed information on the frequencies of individual sequences in each trajectory detailed in Table S5.

Genotype Analysis Identifies Known, Rare, and Previously Unobserved Sequence Motifs

The 33 sequences identified above (Figures 2 and S9; Table S5) and 2 additional sequences that both heavily codepleted were analyzed for the presence of sequence motifs that have been previously shown to robustly inhibit subtype B RTs *in vitro* and to suppress viral replication in cell culture.[7,9–13,22] The FASTAptamer-Search function of the FASTAptamer[24] toolkit was used to search for degenerate sequence motifs, and Mfold[27] was used to generate secondary structure predictions. Although Mfold is unable to predict pseudoknot motifs, we reasoned that it would help provide structural evidence for UCAA and (6/5)AL motifs and could help identify aptamers with novel motifs. Applying this approach with relaxed search constraints identified the three major secondary structural motifs known to bind HIV-1 RT—pseudoknot, (6/5)AL, and UCAA—within most, but not all of these 35 sequences.

FASTAptamer-Search identified ten sequences as F1Pk (Table S6), including the two 70N sequences noted above as having codepleted significantly (70N 2 and 70N 3). The F1Pk motif is characterized by the string UCCG-$N_{7/8}$-CGGGANAAN$_{\geq 3}$, where N refers to any nucleotide, and $N_{\geq 3}$ refers to a segment that base pairs with at least three connector nucleotides to form stem II (Figure 2B).[4–7] Some of these F1Pk-like aptamers diverged slightly from the expected sequence motif definition, and their enrichment patterns appear to reflect their specialized characteristics. For example, 70N 27 and 70N 73 contained only two potential base pairs in stem II. They also showed the strongest enrichment in the EHO (HIV-2) trajectory, potentially allowing this variation of the F1Pk motif to maximize contacts with that particular RT. Similarly, although nine of the ten F1Pk sequences contain a 7 or 8 nt connector, 70N 144 contains a 10 nt connector. The strong enrichment of this sequence in all of the trajectories, including the nitrocellulose-binding population, indicates that it may be a selection parasite rather than a high-affinity RT binder.

The UCAA motif is minimally defined by a 4 nt UCAA bulge flanked by AC/GU closing base pairs on one end and by a stem that is interrupted by a single unpaired U on the other end (Figure 2D).[22] Searching for the UCAA motif identified four sequences, two of which (80N 16 and 80N 148) fully conformed to the motif definition. 80N 16 is identical to aptamer 80.103, which had been identified previously and shown to inhibit HXB2 RT *in vitro* and to suppress viral replication in cell culture.[22] The core element within 80N 148 was validated through aptamer truncation and RT inhibition analysis (Figure S11).

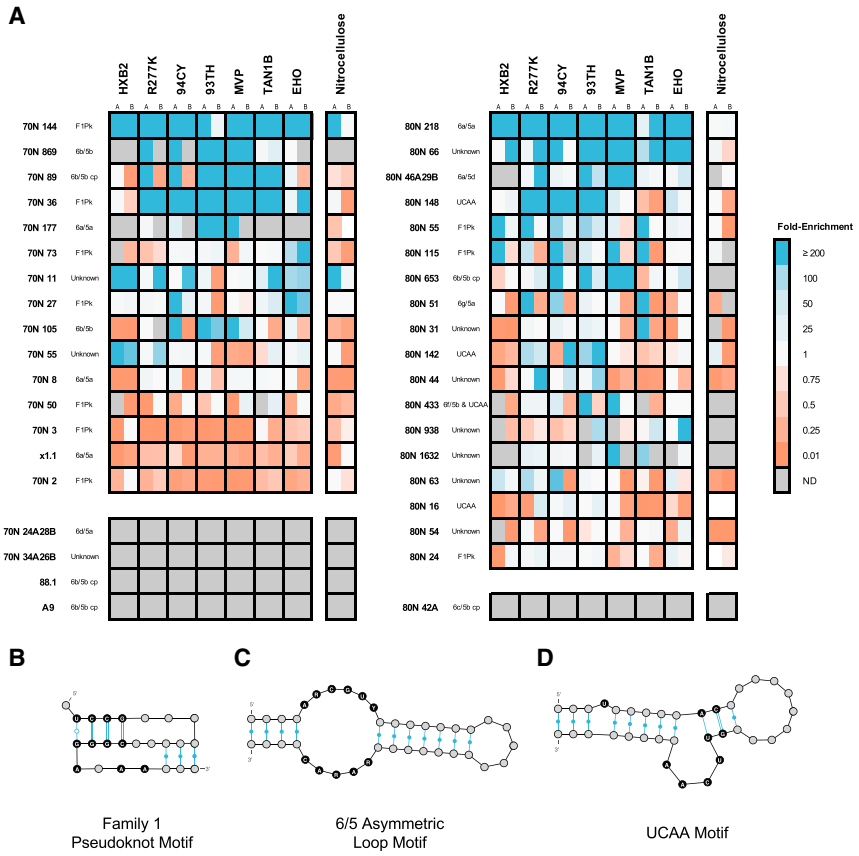

Figure 2. Coenrichment Analysis Identifies Candidate Broad-Spectrum Aptamers

(A) A heatmap of sequence fold-enrichment from the round 14 starting library of candidate aptamers depicts enrichment (blue) or depletion (orange) in each replicate selection trajectory (A or B) and in the nitrocellulose-binding population. Aptamers are grouped by 70N (left set) or 80N (right set) and are sorted top to bottom by decreasing enrichment, averaged across all RT targets. Sequences included in the characterization but that were not detected (ND) in either round 14 or 17 and therefore did not have a enrichment value are colored in gray. Motif names are included to the right of the aptamer identity. Schematic depictions of the secondary structures of the major RT-inhibiting motifs: (B) family 1 pseudoknot (F1Pk), (C) (6/5)AL, and (D) UCAA. Secondary structures were generated using VARNA.[26]

The UCAA elements in the other two identified aptamers were within non-canonical structural contexts and may only superficially resemble the UCAA motif. Aptamer 80N 142 contained the sequence UCAACU but presents the internal CAAC as the 4 nt bulge, rather than the UCAA portion, and both flanking U's are predicted to pair within stems. Nevertheless, this sequence also contained the downstream unpaired U and upstream AC/GU base pairs characteristic of the motif. Although the fourth sequence (80N 433) contained a UCAA motif, it was predicted to present this sequence either as a tetraloop capping an interrupted helix or as a part of a 7 nt bulge (GUUCAAA), neither of which conforms to the canonical structural definition of the UCAA.

The (6/5)AL motif is characterized by the presence of six unpaired nucleotides (ARCGUY) opposite five unpaired nucleotides (RARAC) in an asymmetric loop embedded within a stem (Figure 2C), where R is any purine and Y is any pyrimidine. Of the 16 loop combinations that fit this definition, 6a/5a (AACGUU/GAAAC) and 6b/5b (AGC GUC/AAGAC) variants accounted for >98% of all (6/5)AL motifs in the 70N round 14 library, along with a small fraction of additional minor variants.[7] Searching the candidate sequences for the (6/5)AL motif identified eight sequences that fit the consensus. The 6a/5a variation was present in three sequences (70N 8, 70N 177, and 80N 218). Although most of the previously identified (6/5)AL aptamers use portions of the 80N constant region to form the motif,[7] 80N 218 contained the motif entirely within the aptamer's randomized region. Four aptamers containing the 6b/5b variation of the motif were also identified, with two in the common circularly permuted form (70N 89 and 80N 653) and two in the less common, non-permuted form (70N 105 and 70N 869). A circularly permuted 6c/5b variant that contained the motif within the randomized region was also found (80N 42A). The 6c/5b combination is exceedingly rare, having been previously observed at less than 0.1% of the 70N round 14 population.[7] To validate these motif identifications, RNA 3′ boundary determination for the aptamer:RT complex and inhibition assays with truncated variants were carried out for two non-circularly permuted (70N 105 and 70N 869) and one circularly permuted (70N 89) 6b/5b aptamer. All three fully inhibited RT from HIV-1 strain HXB2 when the 3′ end was truncated to only three base pairs beyond the asymmetric loop, irrespective of whether the closing stem was stem I or stem II (Figures S12–S14).

Sequences with no obvious motifs were analyzed for their predicted secondary structures. Four of these contained asymmetric internal loops suggestive of (6/5)AL variants that did not conform to the ARCGUY/RARAC consensus sequence and hence escaped detection in the initial sequence-based screening. Two of these contain known, but extremely rare, variations of the motif, including 6a/5d (AACGUU/UAAAC; non-conforming deviations underlined) in 80N 46A29B and 6d/5a (AACGUG/GAAAC) in 70N 24A28B. These sequence combinations were previously detected in a 70N library with frequencies of less than 0.6% (6a/5d) and 0.08% (6d/5a) of all (6/5)AL reads.[7] The other two contained previously unobserved variants of the (6/5)AL motif, including the newly termed 6f/5b (AGCGUA/AA GAC) in 80N 433, which is flanked by AG/CC closing pairs in stem I, and 6g/5a (AGCCUC/GAAAC) in 80N 51. The observation of a

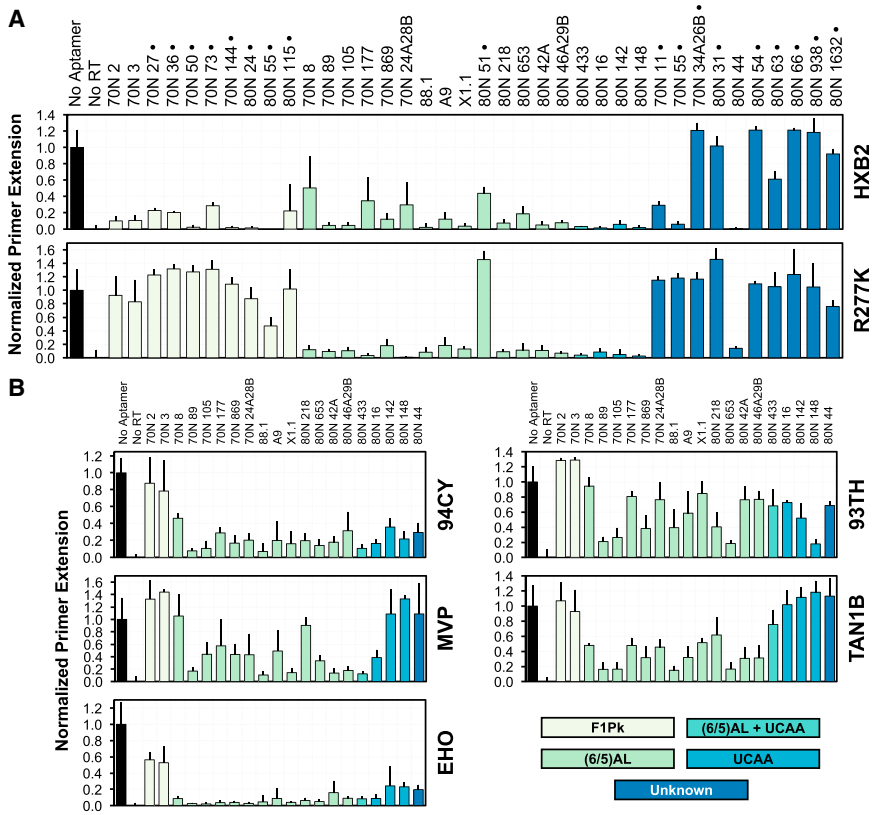

Figure 3. RT Inhibition Assays Reveal Broad-Spectrum Phenotypes

(A) Aptamer-mediated inhibition of the DNA-dependent DNA polymerase activity of RT was determined through primer extension assays against HXB2 RT (top) and an R277K point mutant of HXB2 RT (bottom) for candidate aptamers identified through coenrichment analysis. Aptamers that failed to inhibit both RTs after two independent measurements (marked with bullet points) were eliminated from further examination, with the exception of 70N 2 and 70N 3. (B) Primer extension assays against non-group M:B RTs in the selection panel reveal varying broad-spectrum inhibition. Columns are colored according to aptamer motif. Error bars indicate range for samples assayed in duplicate (marked with bullet points), whereas all other samples are n ≥ 5, and error bars indicate SD.

variant (6/5)AL motif in 80N 433 was especially surprising, as this sequence also contains a non-canonical UCAA bulge, as described above. Minimization of the 80N 433 aptamer, followed by deletion of either the (6/5)AL motif or UCAA bulge, suggested that only the (6/5)AL motif is required for inhibition of HXB2 RT and that the portion containing UCAA is not sufficient for inhibition (Figure S15).

In total, motif analysis of coenriched and codepleted cluster seed sequences, combined with biochemical validation of a subset of these, identified 10 putative F1Pk aptamers, 3 potential UCAA motif aptamers, and 12 (6/5)AL aptamers that include several circular permutations and rare or novel variants. The F1Pk motif comprised the vast majority of the round 14 libraries and continued to be a major component of the final populations despite their overall depletion. One aptamer (80N 433) contained both a cryptic (6/5)AL motif and a dispensable, non-canonical UCAA bulge. Ten additional aptamers neither conformed to previously defined motifs nor showed sequence or structure similarity with each other. Because many of the motif-unknown sequences were also abundant in the nitrocellulose-binding populations, some of these aptamers may be low-fitness species with protein-independent enrichment. Overall, poly-target selection and coenrichment analysis helped reduce the lead candidate space by several orders of magnitude to identify highly coenriched, rare, and unique genotypes that were present within the pre-enriched round 14 libraries. It is unlikely that low-throughput sequencing would have identified these unknown and previously unobserved sequences, as their relative abundance in each library remained low even after three additional rounds of selection.

Broad-Spectrum RT Inhibition Varies with Aptamer Motif

To test whether coenrichment against multiple, divergently related protein targets was an indication of broad-spectrum recognition across the panel of RTs, we assayed the 35 cluster-representing aptamers for inhibition of the DNA-dependent DNA polymerase (DDDP) activity of RT using primer extension assays. Three previously characterized 70N (6/5)AL aptamers (88.1, A9, and x1.1) were included as inhibition controls. Aptamers A9 and 88.1 contain a circularly permuted 6b/5b motif and enriched along many selection trajectories, despite being notably absent from sequences obtained here for the round 14 library. Aptamer x1.1 contains a 6a/5a motif and was the most abundant sequence in the 70N round 14 library,[7] yet it was among the most depleted sequences in the round 17 populations. The vast majority of aptamers containing known motifs robustly inhibited RT from strain HXB2 (Figure 3A, top), which is very closely related (98.9%) to the BH10 strain used to pre-enrich these libraries originally.[6] In contrast, only three of the aptamers without recognizable structural motifs inhibited RT from HXB2 (70N 11, 70N 55, and 80N 44), suggesting that the other candidates with unknown structures may have been enriched for binding to nitrocellulose, that they bind RT surfaces that do not interfere with DNA polymerization, or that they are selection parasites.

The R277K point mutant of RT from HXB2 served as an initial surrogate for evaluating broad-spectrum inhibition. The K277 polymorphism is prevalent among sequenced strains and was present in five of the seven RTs used in these selections, so we reasoned that true broad-spectrum aptamers should be able to inhibit the

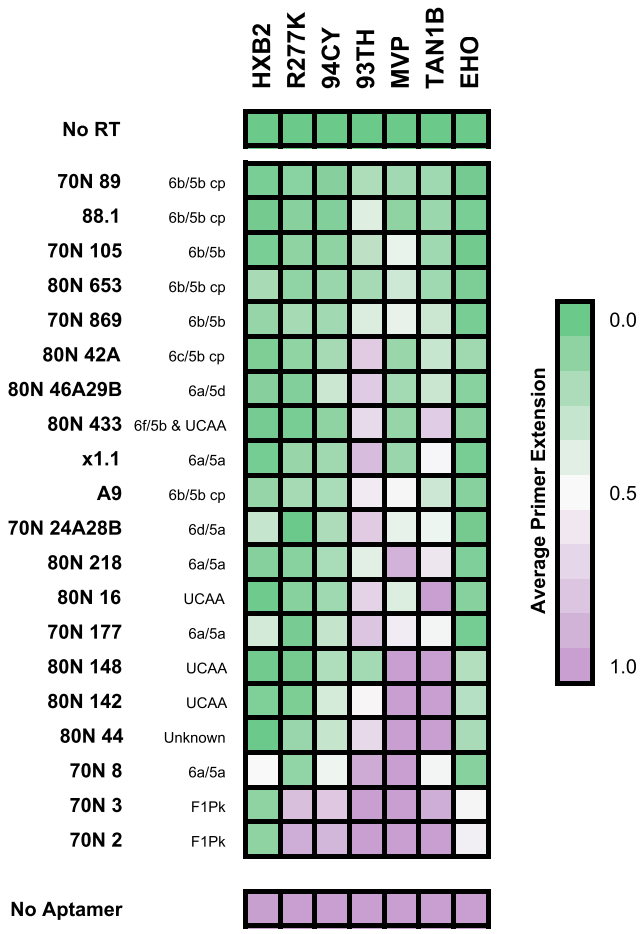

Figure 4. Inhibition Profiles Reveal Motif-Dependent Broad-Spectrum Inhibition

Aptamers are sorted top to bottom by decreasing average inhibition, as measured by primer extension, against the panel of RTs used in the selection. Sorting in this manner reveals a pattern of biochemical RT inhibition corresponding to motif identity. (6/5)AL motifs, particularly the 6b/5b variant, demonstrated the strongest average inhibition against the tested RTs. UCAA motifs and the one previously unidentified aptamer showed variable RT inhibition outside of group M, and F1Pks showed no RT inhibition outside of group M:B.

R277K RT. When all 38 aptamers were tested for inhibition of R277K, 18 of these inhibited both HXB2 and R277K (Figure 3A, bottom). The (6/5)AL and UCAA motif aptamers demonstrated strong inhibition of R277K, with the exception of 80N 51, which weakly inhibited RT from HXB2 and failed to inhibit the point mutant. This aptamer is a previously unobserved 6g/5a variation of the (6/5)AL motif and experienced a mix of both strong depletion and enrichment, often against the same target in replicate selection trajectories. Its coenrichment may therefore reflect the stochastic nature of the selection rather than a true positive coenrichment signal. Of the three aptamers of unknown structures that inhibit HXB2, only aptamer 80N 44 inhibits R277K. As expected, the F1Pk aptamers uniformly failed to inhibit.

When the 18 aptamers that inhibited both HXB2 and R277K were evaluated for inhibition of the panel of RTs used in the selection (Figures 3B and 4), the (6/5)AL and UCAA motif aptamers were consistently broad spectrum. Among the (6/5)AL aptamers, 70N 89 exhibited robust broad-spectrum inhibition of DDDP activity across the primate lentiviral RT panel; to a slightly lesser degree, aptamers 70N 653 and 88.1 also inhibited broadly across the panel. These three aptamers all carry 6b/5b motifs. Aptamer A9, which also carries a 6b/5b motif, showed less inhibition and greater variability across the panel, potentially because of non-productive contributions of sequences surrounding the motif. Aptamer 70N 105, which carries a non-circularly permuted form of the 6b/5b motif, also exhibited a moderate to strong inhibition profile, as did the 6c/5b variant (80N 42A), which is a single-nucleotide change from the 6b/5b motif. Other variations of the (6/5)AL motifs showed no discernible pattern of inhibition across the panel. In particular, 80N 433, which contains both a (6/5)AL and a UCAA motif, behaved most like x1.1 in that it inhibited RTs from 94CY, MVP, and EHO. RT from 94CY and EHO were inhibited more or less uniformly by all (6/5)AL aptamers tested, but inhibition was more variable for RTs from 93TH, MVP, and TAN1B. Aptamers that carry UCAA motifs inhibited RTs from 94CY and EHO and exhibited mixed behavior against RTs from 93TH and MVP. Aptamer 80N 148 moderately inhibited RT from 93TH, but it failed against RT from MVP, while aptamer 80N 16 demonstrated the opposite pattern. All three UCAA aptamers inhibited RT from HIV-2 (EHO) to an extent that is comparable to that observed for the (6/5)AL aptamers, but they all failed to inhibit RT from TAN1B. The unknown aptamer, 80N 44, was only moderately broad spectrum, inhibiting RTs from 94CY and EHO RTs, but none of the other RTs from non-subtype B lentiviruses. 3′ boundary determination and truncation experiments with 80N 44 against HXB2 RT identify a minimized 54 nucleotide sequence predicted to fold as a stem, interrupted with bulges and a (4/2) asymmetric loop, and capped with a six nucleotide loop (Figure S16). The control F1Pk aptamers weakly inhibited RT from EHO, which is the only RT outside the HIV-1 subtype B to contain R277, but they failed to inhibit RTs from the other non-subtype B lentiviruses (Figure 3B).

Sorting the aptamers by their average RT inhibition reveals a clear correlation of inhibition profiles with secondary structural motifs (Figure 4). Taken together, these data indicate that the (6/5)AL and UCAA motifs are capable of inhibiting a broad collection of non-subtype B RTs and that several 6b/5b variants are capable of robust inhibition against every RT in our selection panel. Although the UCAA and unknown motifs show limited inhibition outside of group M subtypes, they are potent inhibitors of the HIV-1 subtype A and B RTs tested here.

Conversion of (6/5)AL Variants to the Canonical 6b/5b Improves RT Inhibition

Aptamers 88.1 (6b/5b), 80N 42A (6c/5b), and 80N 433 (6f/5b) all carry 6b/5b motifs or single-nucleotide variations, and they represent

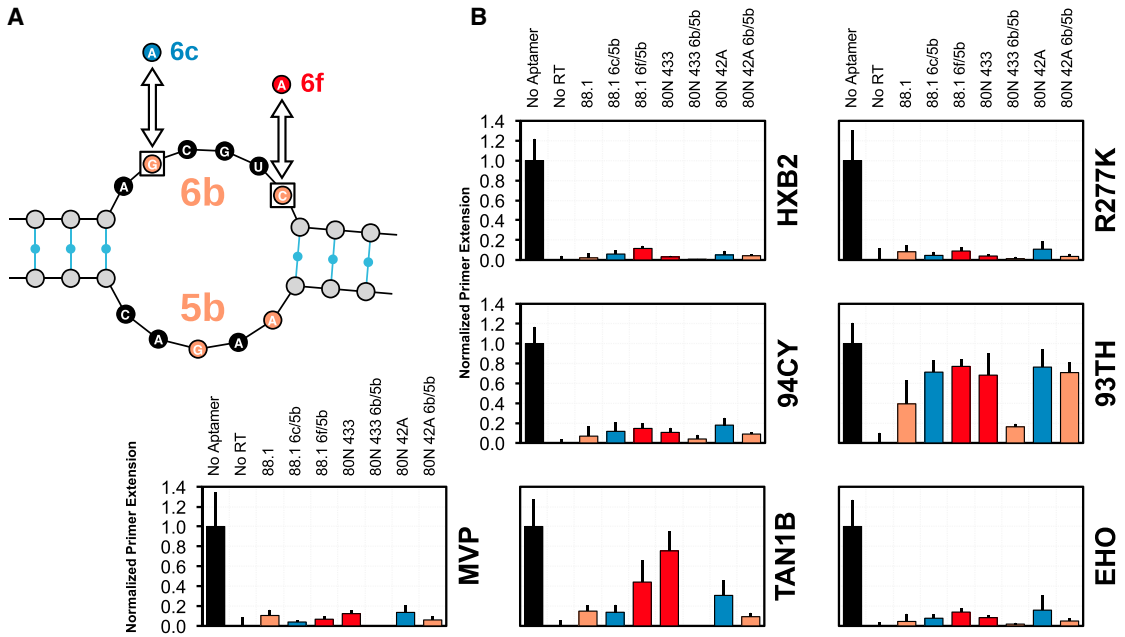

Figure 5. Conversion of Exemplary (6/5)AL Aptamers to the 6b/5b Motif Improves Their Broad-Spectrum Biochemical Inhibition Profile

(A) Single-nucleotide conversions separate 6c/5b (blue) and 6f/5b (red) motifs from the 6b/5b motif (orange). Aptamer 88.1, which contains the 6b/5b motif, was converted to a 6f/5b or 6c/5b and assayed for changes in inhibition against RTs in the selection panel. Conversely, 80N 433 (a 6f/5b aptamer) and 80N 42A (a 6c/5b aptamer) were converted to 6b/5b. (B) Conversion toward the 6b/5b motif uniformly improved biochemical inhibition, whereas conversion away reduced inhibition in most cases. Mean values are shown ($n \geq 5$), and error bars indicate SD.

a gradient of inhibitory potency against RTs from non-B clades. To assess the relative contributions of nucleotide composition within and outside the asymmetric loop, we converted aptamer 88.1 from 6b/5b to 6f/5b and 6c/5b (Figure 5A) and each of the other two into canonical 6b/5b forms. These modifications are single-nucleotide changes to interconvert AGCGUC (6b) to either AGCGUA (6f) or AACGUC (6c), or vice versa. Establishing a canonical 6b/5b structural context for 80N 433 also required an A to G substitution immediately upstream of the 6b element to stabilize the flanking stem. The three original aptamers and the four variants were assayed for inhibition of RTs from HXB2, R277K, and five non-B clades (Figure 5B). Conversion of 88.1 away from the 6b/5b variant had little effect on the overall inhibition profile, with the exceptions of partial loss of inhibition for RTs from 93TH and TAN1B. In contrast, conversion of 80N 433 to 6b/5b (80N 433bb) dramatically increased its inhibitory potency, especially for RTs from 93TH, MVP and TAN1B, making 80N 433bb the strongest broad-spectrum inhibitor among all aptamers examined in this study. Conversion of 80N 42A to 6b/5b also improved its performance against the panel, with lowered mean primer extension values, albeit to a lesser degree than for 80N 433. Taken together, these data suggest that the exact composition of the 6 nt bulge of the (6/5)AL loop is important for broad-spectrum binding, that flanking sequences contribute directly or indirectly to net inhibition, and that the terminal C of the 6 nucleotide bulge, present in both 6b and 6c variants, may be especially important for establishing productive molecular contacts, particularly for RTs from 93TH and TAN1B.

Broad-Spectrum Aptamers Inhibit Outside of the Selection Panel

We reasoned that aptamers capable of inhibiting phylogenetically diverse primate lentiviral RTs likely interact with conserved features that would also be present in RTs that were not included in the polytarget selection panel. Anti-RT aptamers with broad-spectrum ability are therefore expected to bind and inhibit RTs that were not part of this "training set." The aptamers chosen for this analysis were the most potent representatives of the three structural motifs that inhibited outside of subtype B: the 6b/5b converted form of aptamer 80N 433 (80N 433bb), a UCAA aptamer (80N 148), and the putative (4/2)AL motif (80N 44). The RTs for this assay sample two additional subtypes from HIV-1 group M and one from SIV_{CPZ}. The group M RTs included a subtype C (98CN), the predominant form of HIV-1, and a circulating A/D recombinant form (92UG) for which the *pol* gene encoding RT groups within subtype D. The SIV_{CPZ} RT is from the US strain, derived from the chimpanzee species *Pan troglodytes troglodytes* ($SIV_{CPZ}Ptt$), and is more evolutionarily related to HIV-1 group M subtypes than the TAN1B SIV strain used in the selection panel ($SIV_{Cpz}Pts$) (Figure S1).[23] Against the RT from subtype D (92UG), the UCAA aptamer showed moderate inhibition, and the 6b/5b aptamer showed complete inhibition (Figure 6). When assayed against the RT from subtype C (98CN), all three aptamers showed moderate inhibition, with the 6b/5b aptamer exhibiting virtually complete inhibition of the DDDP activity. Finally, only the 6b/5b aptamer inhibited the RT from SIV_{CPZ} (US). These results provide further evidence of the ability of the UCAA and unknown motif to

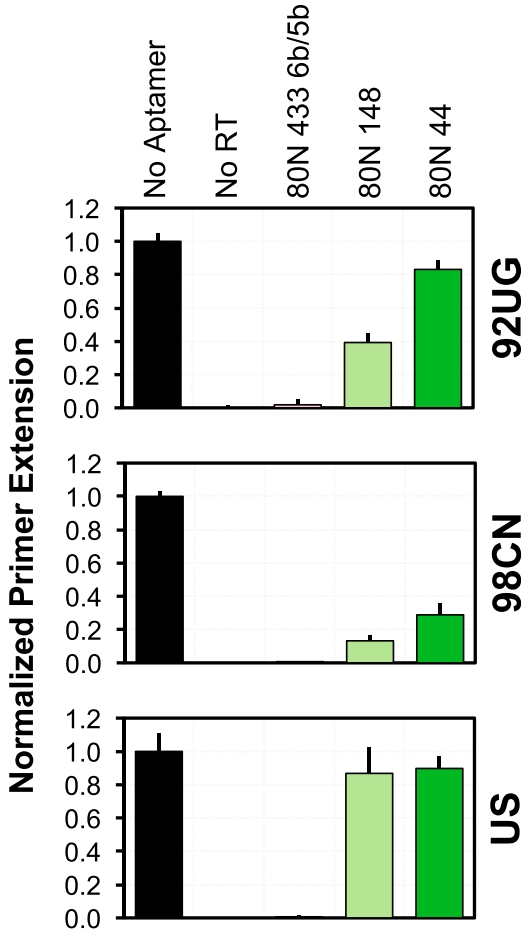

Figure 6. Broad-Spectrum Aptamers Are Capable of RT Inhibition Outside of the Selection Panel

Aptamers representing the three motifs with non-subtype B RT inhibition were tested against RTs from two group M strains (92UG and 98CN) and an SIV strain (US). 92UG, a circulating recombinant form of HIV-1 group M whose RT groups with subtype D, is inhibited moderately by the UCAA motif aptamer and robustly by the 6b/5b aptamer. RT from 98CN, a group M:C strain, is inhibited by all three aptamers tested, including 80N 44 (unknown motif). RT from the US strain of SIV_{CPZ}*Ptt* is inhibited only by the 6b/5b aptamer. Mean values are shown ($n \geq 5$), and error bars indicate SD.

inhibit non-subtype B RTs and of the 6b/5b motif to strongly inhibit RT from phylogenetically diverse primate lentiviral strains.

Broad-Spectrum Anti-RT Aptamers Bind with Low Nanomolar Affinity

We hypothesized that the observed patterns of sequence enrichment and enzymatic inhibition above should reflect relative affinities for each aptamer-RT combination. For example, because modifying aptamer 80N 433 into a canonical 6b/5b form improved its inhibition of RTs from 93TH and TAN1B RT, the modified aptamer is expected to exhibit improved affinity for these RTs. Apparent dissociation constants for a number of aptamer-RT pairs were determined by a nitrocellulose filter binding assay (Table 1; Figure S17). As expected, aptamer 70N 2 (F1Pk) bound well to RT from HXB2 (dissociation constant [K_D] ≈ 110 nM) but showed no discernable affinity for the R277K point mutant, consistent with its inhibition patterns (Figure 3A). Furthermore, its affinity for RT from HXB2 was notably weaker than affinities observed for the broad-spectrum aptamers tested here, consistent with the moderate depletion of aptamer 70N 2 in the HXB2 trajectory and its powerful depletion in each of the others (Figure 2; Table S5). Dissociation constants for all of the other aptamers were in the low nanomolar range (<100 nM) for binding to HXB2. Because these assays were all performed at the same time using the same protein preparation, we conclude that the affinity of aptamer 80N 433bb for RT from HXB2 is 5-fold improved relative to that of the pseudoknot aptamer 70N 2. All of the broad-spectrum aptamers showed reduced affinity for the R277K mutant, relative to their affinities for RT from HXB2. For the RTs from non-subtype B lentiviruses, relative binding affinities among the broad-spectrum aptamers correlated with their inhibition profiles. In particular, K_D values for the 6b/5b variant of 80N 433 were in the low nanomolar range across the RT panel, and this aptamer uniformly bound more strongly to each RT than did any of the other aptamers. Affinity improvements associated with converting the original 80N 433 from 6f/5b to 6b/5b ranged from approximately 3-fold for HXB2 and 93TH to 13-fold for TAN1B, illustrating the variable contributions of these nucleotide changes upon the RT-aptamer interactions.

Broad-Spectrum Anti-RT Aptamers Suppress Viral Replication in Cell Culture Assays

To determine whether aptamers that demonstrate broad-spectrum activity *in vitro* also inhibit diverse HIV in a biological context, we adapted an assay that we had previously developed for monitoring aptamer-mediated inhibition of HIV replication in cell culture.[12,13,28] Briefly, transfection of plasmids encoding a replication-deficient HIV reporter virus and the glycoprotein from vesicular stomatitis virus (VSV-G) leads to production of virus that are competent for a single cycle of replication and for which transfection and infection efficiencies can both be measured using the virally encoded EGFP. Co-transfection of aptamer-expressing plasmid simultaneously with viral plasmids can lead to packaging of the aptamer into the virus during assembly, inhibition of reverse transcription in the target cells, and loss of infectivity that can be measured by a loss of fluorescence signal in the target cells. To incorporate phylogenetically diverse RT subtypes into this assay, we first built and evaluated proviral plasmids to express several RTs from our poly-target selection panel (HXB2, R277K, 93TH, 94CY, and MVP) such that only the RT segments differed in each construct.[13] This assay was used to evaluate viral inhibition by aptamers that demonstrated broad-spectrum RT inhibition *in vitro* by co-transfecting various combinations of proviral and helper VSV-G plasmids with aptamer or control plasmids, collecting the pseudotyped virus and determining the percentage of EGFP-positive cells after infection of fresh 293FT cells (Figure 7). Infectivity was normalized to p24 levels determined by ELISA. As observed previously,[13] aptamer 70.05 (an F1Pk pseudoknot) strongly inhibited infectivity of virus carrying the HXB2 RT but not the R277K point mutant or any of the non-subtype B RTs. In contrast, aptamers

Table 1. Apparent Binding Affinity (K_D) of Broad-Spectrum RT Aptamer Inhibitors

	HXB2	R277K	94CY	93TH	MVP	TAN1B	EHO
70N 2	110 ± 20	>>300	–	–	–	–	–
80N 44	60 ± 12	190 ± 51	30 ± 9	58 ± 17	–	–	–
80N 148	74 ± 17	150 ± 42	55 ± 13	13 ± 3	–	–	–
80N 433	59 ± 23	–	–	22 ± 6	–	210 ± 38	–
80N 433bb	22 ± 4	38 ± 7	29 ± 8	7 ± 1	39 ± 8	16 ± 2	34 ± 9

Values are listed in nanomolar with SD from triplicate assays. Binding curves are provided in Figure S17.

80N 433 and 80N 433bb inhibited infectivity of all recombinant viruses in the panel. Aptamers 80N 148 and 80N 44 demonstrated a variable pattern against the non-subtype B RTs. Both inhibited replication by viruses carrying RT from 94CY but only 80N 148 inhibited virus carrying RT from 93TH, even though the RTs from 94CY and 93TH both group within subtype A and are 91.4% identical (98.2% similar). Neither 80.148 nor 80.44 inhibited viruses carrying RT from the MVP5180 strain of HIV-1 group O. These results are consistent with our biochemical inhibition results and closely mirror our previous observations for inhibition by the major anti-RT motifs in cell culture.[13]

DISCUSSION

Recent advances in aptamer technology have enabled increased selection throughput and high-resolution analysis of selection outcomes.[29,30] Microfluidic[31] and multiplexed selection platforms[32,33] facilitate efficient and simultaneous selection against numerous targets, and emulsion methods that encapsulate single genotypes into "monoclonal aptamer particles" can readily partition or sort according to phenotype.[34,35] Post-selection, HTS has empowered optimization of candidate aptamers on the basis of round-to-round enrichment of sequences and by providing large datasets that allow powerful bioinformatic analyses of sequence, structure, and function relationships.[7,36–38] The use of HTS for analyzing aptamer selection outcomes has been bolstered by a number of specialized software packages, such as FASTAptamer,[24] Aptani,[39] and AptaSUITE.[40] In addition to advances in selection methodology and candidate identification, high-throughput aptamer characterization platforms can screen thousands of aptamers simultaneously[41] and can directly link genotype to phenotype if performed on a sequencing platform.[42,43] Here we combined HTS with multiplexed selections against a diverse panel of recombinant RTs. We applied these technologies to elicit specialized binding and inhibition phenotypes (cross-reactivity) from well-characterized and pre-enriched aptamer libraries. Furthermore, we sequenced negative selection populations and performed our positive selections in duplicate. The combination enabled coenrichment analysis of multiple selection trajectories, nuanced with data from duplicate and negative selections. This strategy efficiently narrowed the number of potential candidates to an examinable amount, allowing us to identify highly potent RNA broad-spectrum inhibitors of primate lentiviral RTs among these candidates. Interestingly, we observed substantial variation between replicate selection trajectories, highlighting the inherent stochasticity of selections and benefit of providing multiple opportunities for rare, yet favorable, phenotypes to emerge.

Other selection approaches have previously been used to identify cross-reactive aptamers or to exploit branched selections. In "toggle SELEX,"[44] the target of a single-selection trajectory is alternated, or "toggled," between rounds; this approach was used to identify inhibitors of human and porcine thrombin and later to identify broadly reactive aptamers targeting whole bacterial cells.[45] In another approach, single-pot selections against numerous targets were used to identify cross-reactive aptamers against several M-types of *Streptococcus pyogenes*[46] and against HA proteins from multiple strains of influenza A.[47] Although both of these methods are powerful (alternating or simultaneous targets), they rely on a single evolutionary trajectory and lack the target-specific information that can inform the aptamer selection and design process. Recently, Dupont et al.[48] reported on a clever branched selection approach against alanine point mutants of serpin plasminogen activator inhibitor-1 (PAI-1). Using a library previously selected against wild-type PAI-1, those authors performed one additional round of selection against a panel of ten targets, in parallel, followed by HTS, to identify aptamer binding site preferences. Unlike the poly-target selection described here, the pre-enriched library used by Dupont et al. had not been saturated. In the original selection against PAI-1, enrichment of the library was detected after five rounds and proceeded for a total of eight rounds.[49] Rather than using the heavily enriched library from round 8, the branched selection began with round 5, allowing a greater diversity of aptamers to emerge.

The poly-target approach used pre-enriched libraries to simultaneously explore a wider sequence space than available in a traditional aptamer directed evolution strategy. Interestingly, abundance, enrichment, and coenrichment alone were not strong predictors of fitness in the poly-target selection performed here. Highly abundant sequences in the starting libraries depleted across most selection trajectories yet retained a major presence within the round 17 populations. In contrast, most of the 6b/5b variants that enriched through the selection were so rare in the starting populations that despite their large fold enrichment, they remained as a relatively small percentage of the populations and could only be reliably identified through HTS. Coenrichment was slightly more predictive of broad-spectrum phenotypes after removing aptamers that enriched against nitrocellulose alone. Nevertheless, several F1Pk aptamers demonstrated enrichment

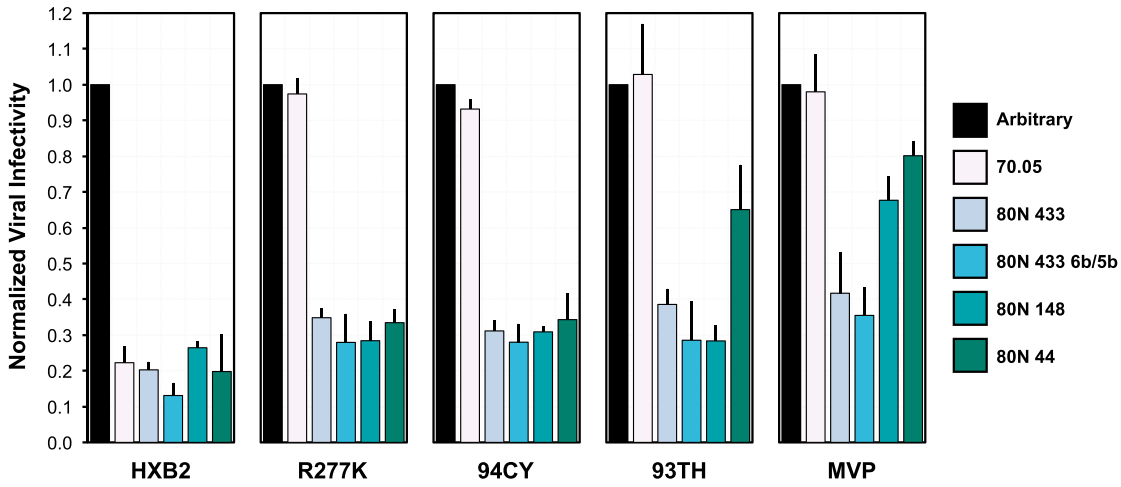

Figure 7. Broad-Spectrum Anti-RT Aptamers Suppress Viral Replication in Biological Assays

A non-inhibitory RNA ("arbitrary"), a previously characterized F1Pk aptamer (70.05), and several broad-spectrum aptamers identified through poly-target selection were assessed for their ability to suppress virus in a single-cycle infectivity assay.

across several trajectories despite their lack of broad-spectrum inhibition. The combined use of coenrichment and codepletion analysis of sequence clusters identified sequences that experienced mixed enrichment and depletion, either across trajectories or between replicates. The most productive analytic strategy for the present datasets combined each of these approaches with careful curation on the basis of sequence and structural motifs established from previous investigations. The poly-target approach may be broadly applicable for any combinatorial selection or directed evolution strategy that seeks to identify broad-spectrum behavior given an appropriate phenotypic screen.

The primer-template-binding groove in RT extends from between the thumb and fingers domain along the palm to the RNaseH domain. Although the RT amino acid sequence within this groove is among the most highly conserved portions of the protein, natural polymorphisms and subtype-specific variations affect nucleic acid interaction affinity and specificity. The poly-target selection strategy was designed to intentionally select for promiscuity against a family of related targets, rather than specificity for a single target or its point mutants, and it relied on the sequencing depth provided by HTS to identify functionally rare aptamers that enriched from our round 14 starting libraries. We developed and used a coenrichment analysis strategy to efficiently reduce the dataset from more than 100 million sequences to focus on dozens of candidate sequence clusters for further analysis. We were able to identify several rare variants of (6/5)AL motifs and also a previously unknown aptamer inhibitor of HIV-1 group M RTs. Inhibition assays identified the 6b/5b variant of the (6/5)AL motif as an especially potent inhibitor of the DDDP activity of RTs used in the selection panel and several RTs that were not represented in the selection. Conversion of aptamer 80N 433 toward the 6b/5b motif improved its inhibition profile across the panel of RTs and most notably against 93TH, MVP and TAN1B. Furthermore, the UCAA aptamer (80N 148) and aptamer 80N 44 demonstrated inhibition of RT outside of subtype B strains. Follow-up assays correlated *in vitro* inhibition of RTs with binding affinity and suppression of viral replication. As our efforts were focused on identification of broad-spectrum inhibitors, we did not attempt to find strain-specific inhibitors, nor did we closely examine the role of individual nucleotides and their interactions with specific RTs. The wealth of data provided by the poly-target selection approach should, in principle, allow one to look for enrichment exclusive for a particular target, in addition to advancing the broad-spectrum objectives that were the focus of the present study. An intriguing question to be explored in future studies is whether resistance arises from a small number of mutations for "specialist" aptamers (such as the R277K mutation for F1Pk aptamers) and requires significantly more mutations for broad-spectrum aptamers, making such breakout mutation a low-probability event and creating what is sometimes referred to as a high genetic barrier to resistance.

MATERIALS AND METHODS

RT Expression and Purification

DNA encoding the p66 and p51 subunits of each RT (Table S1) was PCR-amplified from previously described pET200/D-TOPO expression vectors.[16] Amplicons were then restriction digest cloned into the pRT-Dual plasmid, a derivative of pETDuet-1 vector (a gift from Stefan Sarafianos).[50] Plasmids expressing RTs from HXB2, R277K, 94CY, and TAN1B used the PpuM1/SacI cloning sites for the p51 subunit and the SacII/AvrII sites for the p66 subunit ("pRTD" series plasmids), whereas RTs from 93TH, MVP, and EHO used the same restriction sites for the p66 subunit but used NotI/SalI for the p51 subunit ("pRTD2" series plasmids). Additional plasmid engineering was performed on the ribosome-binding site upstream of the p66 subunit in the pRTD2 series plasmids to optimize expression. Plasmid inserts were confirmed by Sanger sequencing

(University of Missouri DNA Core Facility) and are available upon request.

RT expression plasmids were heat shock transformed into *E. coli* BL21(DE3)pLysS-competent cells and then incubated overnight at 37°C on LB-agar plates supplemented with selective antibiotic (50 μg/mL streptomycin). Clonal isolates from each plate were recovered and incubated for approximately 16 hr at 37°C with 250 rpm shaking in 10 mL of 2xYT selective liquid media. Cultures were then diluted into 1 L of fresh media, and optical density at 600 nm was monitored until reaching 0.5, whereupon protein overexpression was induced with 1 mM IPTG. Following a 4 hr incubation, samples were centrifuged for 15 min at 4,000 relative centrifugal force (RCF). Supernatants were decanted, and cell pellets were frozen at −80°C until purification. For purification, cell pellets were resuspended in sonication buffer (25 mM Tris-HCl [pH 8.0], 500 mM NaCl, 1 mM PMSF, and 0.15 mg/mL lysozyme) and then subjected to four ultrasonication steps for 30 s on ice, with 2 min of rest on ice in between steps. Cell lysates were then centrifuged for 15 min at 4°C and 12,000 RCF to remove cell debris. Cell extracts were then passed through a 0.45 μm filter to remove insoluble material and applied to a Ni-NTA agarose affinity column (QIAGEN) for His tag purification. Purification was performed according to the manufacturer's protocol with an added high-salt wash (2 M NaCl) to remove any endogenous nucleic acids bound to RTs. Eluted protein samples were pooled and quantified using UV absorbance at 280 nm on a NanoDrop 1000 spectrophotometer (Thermo Fisher Scientific) with estimated extinction coefficient and molecular weight information. Purified proteins were concentrated using Amicon Ultra Centrifugal Filters (Millipore Sigma) and dialyzed into 2× storage buffer (100 mM HEPES [pH 7.5], 100 mM NaCl) using Slide-A-Lyzer cassettes (Thermo Fisher Scientific). RT preps were validated for purity and size by SDS-PAGE and for activity by comparison of primer extension assays against previous preps. Proteins were stored at −20°C after addition of glycerol to 50% (v/v).

Poly-Target Selection

Starting libraries for this work were the round 14 70N and 80N libraries described previously.[6] Double-stranded DNAs from these libraries were transcribed using T7 RNA polymerase, *in vitro* transcription buffer (50 mM Tris-HCl [pH 7.5], 15 mM $MgCl_2$, 5 mM DTT, and 2 mM spermidine), and 2 mM of each ATP, CTP, GTP, and UTP. Reactions were incubated at 37°C for a minimum of 4 hr and halted with the addition of gel loading buffer (95% formamide, 5 mM EDTA, xylene cyanol FF, and bromophenol blue). Transcribed RNAs were purified through denaturing PAGE (6% TBE-PAGE, 8 M urea), and bands corresponding to the expected size were gel-extracted and eluted while tumbling overnight in 300 mM sodium acetate (pH 5.4). Eluates were ethanol precipitated, resuspended in TE buffer (10 mM Tris-HCl [pH 8.0] and 1 mM EDTA), and stored at −20°C until use. RNA concentrations were determined using a NanoDrop 1000 spectrophotometer (Thermo Fisher Scientific). For each trajectory and round of selection, 200 pmol of the transcribed libraries (~1.2×10^{14} molecules, providing thorough oversampling of the diversity present in this pre-enriched library) were resuspended in 100 μL binding buffer (150 mM KCl, 10 mM $MgCl_2$, and 50 mM Tris-HCl [pH 7.5]) and renatured by heating to 65°C and cooling on ice; 40 pmol of the respective RT was then added, and the mixture was incubated on ice for an additional 20 min. Separately, a 25 mm nitrocellulose filter (HAWP02500; Millipore Sigma) was pre-wet with 2 mL binding buffer on a sampling manifold (XX2702550; Millipore Sigma). Immediately before application of incubated RNA:RT complex, the nitrocellulose filter was washed again with 1 mL of binding buffer under applied vacuum. RNA:RT complex was then applied to filter under vacuum and washed with 1 mL of binding buffer. Suction continued for 10 min. The filter was then removed and incubated in extraction buffer (8 M urea, 50 mM NaCl, and 10 mM EDTA). RNA was recovered by phenol:chloroform extraction of the filter and ethanol precipitation. Recovered RNA was reverse-transcribed using ImProm-II Reverse Transcriptase (Promega) and PCR-amplified to repeat the selection process or for HTS (see below). Prior to round 15, transcribed round 14 libraries were incubated with a thin strip of nitrocellulose for several minutes to subtract non-specific binders, and RNA was extracted and purified as described above, with the exclusion of the RT binding and partitioning steps. Nitrocellulose-binding RNAs were recovered and reverse-transcribed for HTS, while nitrocellulose-subtracted RNAs were used for independent selections.

HTS and Bioinformatics Analysis

Libraries were prepared for sequencing using a series of PCR steps to add Illumina adapters and sequencing indices for multiplexing of the 70N and 80N libraries as previously described.[7] Sequencing was performed on an Illumina HiSeq2000 (University of Missouri DNA Core Facility). Populations were demultiplexed to identify and parse the 5′ and 3′ constant regions. Data pre-processing was performed using cutadapt[51] to trim 5′ and 3′ constant regions from sequences and to discard any uncut sequences or sequences not within ±3 of the expected size (70 or 80) after trimming. Trimmed sequences were then filtered for high-quality reads using FASTQ quality filter from the FASTX-Toolkit (http://hannonlab.cshl.edu/fastx_toolkit/). Quality filtering eliminated a sequence if a single position had a Phred quality score of less than 20. Trimmed and quality filtered sequences were then processed using the FASTAptamer toolkit[24] to count and normalize sequence reads (FASTAptamer-Count), calculate fold enrichment from round 14 to round 17 (FASTAptamer-Enrich), compare sequence frequencies across populations (FASTAptamer-Compare), group related sequences into clusters (FASTAptamer-Cluster), and search for known sequence motifs (FASTAptamer-Search). Custom scripts (open source and available at https://github.com/FASTAptamer/PolyTarget) were written in Perl to perform coenrichment analysis, to map sequences onto their round 14 identity, and to recluster the sequences as described in the results. RNA secondary structures were predicted using the mfold webserver[27] and depicted using VARNA: Visualization Applet for RNA.[26]

Aptamer Generation

Oligonucleotides for DNA transcription templates were ordered from Integrated DNA Technologies and ligated as previously

described.[52] Ligated oligonucleotides were then PCR-amplified with Pfu DNA polymerase, and primers containing the T7 promoter and the remainder of the constant region that was not included in the oligonucleotides. Amplification products were verified for size using agarose gel electrophoresis. Run-off transcription reactions using T7 RNA polymerase and RNA extraction and purification were performed as described above for transcription of poly-target libraries. RNAs were refolded by heating to 65°C and cooling on ice prior to use.

Primer Extension Assays

DDDP activities of RTs were assayed using a 31 nt DNA template (5′ CCATAGATAGCATTGGTGCTCGAACAGTGAC 3′) and a complementary, 5′-Cy3-labeled 18-nucleotide DNA primer (5′ Cy3-GTCACTGTTCGAGCACCA 3′) as previously described.[22] In short, 20 nM of RT and 100 nM of aptamer (omitted for "no aptamer" control) were pre-incubated on ice for 10 min in extension buffer (50 mM Tris-HCl [pH 7.5], 50 mM NaCl, and 5 mM $MgCl_2$). Then 10 nM primer, 20 nM template, and 100 μM of each dNTP were added immediately before incubation at 37°C for 10 min. Reactions were halted with the addition of gel loading buffer (95% formamide, 5 mM EDTA, xylene cyanol FF, and bromophenol blue) and analyzed by denaturing PAGE (10% TBE-PAGE, 8 M urea). Gels were scanned on a Typhoon FLA9000 imager (GE Healthcare) and quantified using Multi Gauge software (Fujifilm) for fraction of primer extended. Primer extension values were then normalized by subtracting the mean "no RT" value for the respective RT and multiplying by a normalization factor that defines 100% extension as the mean extension in the "no aptamer" control.

Aptamer:RT 3′ Boundary Determination

In vitro transcribed and purified RNA was treated with Antarctic phosphatase (Fermentas) to remove the 5′ terminal phosphate and subsequently labeled with T4 polynucleotide kinase in the presence of γ-^{32}P-labeled ATP (PerkinElmer). Radiolabeled RNA was gel-purified by denaturing PAGE as described for transcription of libraries. RNase T1 digestion was performed by incubating thermally renatured RNA (>10^6 CPM) with 40 units of RNase T1 (Thermo Fisher Scientific) in digestion buffer (25 mM sodium citrate [pH 5.0], 6 M urea) for 5 min at 55°C. T1 digestion was halted with the addition of gel loading buffer. Alkaline hydrolysis was performed by incubating RNA in 50 mM sodium carbonate (pH 9.0) at 90°C for 10 min. Hydrolysis was halted upon addition of 300 mM sodium acetate (pH 5.0) and were then ethanol precipitated and resuspended in H_2O. Aptamer:RT 3′ boundary was determined by incubating 50 pmol RNA with 100 pmol HXB2 RT and partitioning the bound complexes as described above for the poly-target selection. RNAs were recovered from the filter and resolved on a denaturing polyacrylamide gel (15% TBE-PAGE, 8 M urea).

Affinity Constant Determination

Affinity constants (K_D values) were determined by a radiolabeled binding assay. Approximately 15,000–20,000 CPM of labeled and refolded RNA was incubated with varying concentrations of RT (0.1–1000 nM or without RT to determine background binding) in binding buffer (50 mM Tris-HCl [pH 7.5], 140 mM KCl, 1 mM $MgCl_2$, and 0.1 μg/mL BSA) and allowed to equilibrate on ice for 15 min. Assembled RNA:RT complexes were then partitioned from unbound RNA by passing samples over a nitrocellulose filter (HAWP02500; Millipore Sigma) under vacuum (XX2702550; Millipore Sigma) and immediately washing with 500 μL binding buffer. Radioactivity retained on filters was counted by adding 4 mL of scintillation fluid to filters placed inside of scintillation vials and counted using a liquid scintillation counter. Fraction of RNA bound was calculated by determining the fraction of radioactivity bound and were fit to a one-site, specific binding curve using Prism GraphPad 6.2. Replicates of binding assays were performed using recently prepared single batches of each protein and aptamer for all K_D measurements involving that protein or aptamer, to avoid drift of signal from aging samples or from batch-to-batch variation.

Viral Infectivity Assay

Cell culture, virus production, and evaluation of viral infectivity were carried out as previously described.[13,28] Single-cycle infectivity assays using aptamer-expressing plasmids, pNL4-3-CMV-GFP and pMD-G (VSV-G), were performed by transfecting 293FT cells with polyethylenimine (PEI) in six-well cell culture dishes. All transfections were performed on cells plated the previous day (50% confluence) using PEI at 3 μL/μg DNA, as previously described. Aptamer-expressing plasmids (1,000 ng) were co-transfected with a mixture of pNL4-3-CMV-GFP (150 ng) and pMD-G (50 ng). The medium was changed approximately 12 hr after transfection. Viral supernatant was harvested 48 hr after the post-transfection media change and clarified by centrifugation to remove cellular debris. Cell-free viral supernatant (50 μL) was added to fresh 293FT cells to determine infectivity. Infected cells were collected 24–48 hr post-infection, fixed with 4% paraformaldehyde, and analyzed on an Accuri C6 Flow Cytometer (BD Biosciences) to determine the percentage of infected (EGFP-positive) cells. Infectivity data were normalized to levels of p24 determined by ELISA.

SUPPLEMENTAL INFORMATION

Supplemental Information includes seventeen figures and six tables and can be found with this article online at https://doi.org/10.1016/j.omtn.2018.10.010.

AUTHOR CONTRIBUTIONS

Conceptualization, K.K.A. and D.H.B.; Methodology, K.K.A., M.J.L., and D.H.B.; Software, K.K.A. and J.L.C.; Validation, K.K.A., J.L.C., M.J.L, and P.D.M.N.; Formal Analysis, K.K.A., M.J.L., and D.H.B.; Investigation, K.K.A., J.L.C., M.J.L., P.D.M.N., and A.W.S.; Resources, D.H.B.; Data Curation, K.K.A.; Writing – Original Draft, K.K.A. and D.H.B.; Writing – Review & Editing, K.K.A., J.L.C., M.J.L., P.D.M.N., A.W.S., and D.H.B.; Visualization, K.K.A.; Supervision, K.K.A. and D.H.B.; Project Administration, D.H.B.; Funding Acquisition, D.H.B.

CONFLICTS OF INTEREST

The authors have no conflicts of interest.

ACKNOWLEDGMENTS

We would like to thank Katherine N. Wilsdon for technical assistance. This work was supported by NIH grant R01AI074389 to D.H.B. and by a graduate research assistantship to K.K.A. from the University of Missouri Department of Biochemistry.

REFERENCES

1. Tuerk, C., and Gold, L. (1990). Systematic evolution of ligands by exponential enrichment: RNA ligands to bacteriophage T4 DNA polymerase. Science *249*, 505–510.
2. Ellington, A.D., and Szostak, J.W. (1990). In vitro selection of RNA molecules that bind specific ligands. Nature *346*, 818–822.
3. Li, Y. (2015). A quarter century of in vitro selection. J. Mol. Evol. *81*, 137–139.
4. Tuerk, C., MacDougal, S., and Gold, L. (1992). RNA pseudoknots that inhibit human immunodeficiency virus type 1 reverse transcriptase. Proc. Natl. Acad. Sci. U S A *89*, 6988–6992.
5. Green, L., Waugh, S., Binkley, J.P., Hostomska, Z., Hostomsky, Z., and Tuerk, C. (1995). Comprehensive chemical modification interference and nucleotide substitution analysis of an RNA pseudoknot inhibitor to HIV-1 reverse transcriptase. J. Mol. Biol. *247*, 60–68.
6. Burke, D.H., Scates, L., Andrews, K., and Gold, L. (1996). Bent pseudoknots and novel RNA inhibitors of type 1 human immunodeficiency virus (HIV-1) reverse transcriptase. J. Mol. Biol. *264*, 650–666.
7. Ditzler, M.A., Lange, M.J., Bose, D., Bottoms, C.A., Virkler, K.F., Sawyer, A.W., Whatley, A.S., Spollen, W., Givan, S.A., and Burke, D.H. (2013). High-throughput sequence analysis reveals structural diversity and improved potency among RNA inhibitors of HIV reverse transcriptase. Nucleic Acids Res. *41*, 1873–1884.
8. Held, D.M., Kissel, J.D., Saran, D., Michalowski, D., and Burke, D.H. (2006). Differential susceptibility of HIV-1 reverse transcriptase to inhibition by RNA aptamers in enzymatic reactions monitoring specific steps during genome replication. J. Biol. Chem. *281*, 25712–25722.
9. Joshi, P., and Prasad, V.R. (2002). Potent inhibition of human immunodeficiency virus type 1 replication by template analog reverse transcriptase inhibitors derived by SELEX (systematic evolution of ligands by exponential enrichment). J. Virol. *76*, 6545–6557.
10. Chaloin, L., Lehmann, M.J., Sczakiel, G., and Restle, T. (2002). Endogenous expression of a high-affinity pseudoknot RNA aptamer suppresses replication of HIV-1. Nucleic Acids Res. *30*, 4001–4008.
11. Joshi, P.J., North, T.W., and Prasad, V.R. (2005). Aptamers directed to HIV-1 reverse transcriptase display greater efficacy over small hairpin RNAs targeted to viral RNA in blocking HIV-1 replication. Mol. Ther. *11*, 677–686.
12. Lange, M.J., Sharma, T.K., Whatley, A.S., Landon, L.A., Tempesta, M.A., Johnson, M.C., and Burke, D.H. (2012). Robust suppression of HIV replication by intracellularly expressed reverse transcriptase aptamers is independent of ribozyme processing. Mol. Ther. *20*, 2304–2314.
13. Lange, M.J., Nguyen, P.D.M., Callaway, M.K., Johnson, M.C., and Burke, D.H. (2017). RNA-protein interactions govern antiviral specificity and encapsidation of broad spectrum anti-HIV reverse transcriptase aptamers. Nucleic Acids Res. *45*, 6087–6097.
14. Jaeger, J., Restle, T., and Steitz, T.A. (1998). The structure of HIV-1 reverse transcriptase complexed with an RNA pseudoknot inhibitor. EMBO J. *17*, 4535–4542.
15. Kensch, O., Connolly, B.A., Steinhoff, H.-J., McGregor, A., Goody, R.S., and Restle, T. (2000). HIV-1 reverse transcriptase-pseudoknot RNA aptamer interaction has a binding affinity in the low picomolar range coupled with high specificity. J. Biol. Chem. *275*, 18271–18278.
16. Held, D.M., Kissel, J.D., Thacker, S.J., Michalowski, D., Saran, D., Ji, J., Hardy, R.W., Rossi, J.J., and Burke, D.H. (2007). Cross-clade inhibition of recombinant human immunodeficiency virus type 1 (HIV-1), HIV-2, and simian immunodeficiency virus SIVcpz reverse transcriptases by RNA pseudoknot aptamers. J. Virol. *81*, 5375–5384.
17. Schneider, D.J., Feigon, J., Hostomsky, Z., and Gold, L. (1995). High-affinity ssDNA inhibitors of the reverse transcriptase of type 1 human immunodeficiency virus. Biochemistry *34*, 9599–9610.
18. Kissel, J.D., Held, D.M., Hardy, R.W., and Burke, D.H. (2007). Single-stranded DNA aptamer RT1t49 inhibits RT polymerase and RNase H functions of HIV type 1, HIV type 2, and SIVCPZ RTs. AIDS Res. Hum. Retroviruses *23*, 699–708.
19. Kissel, J.D., Held, D.M., Hardy, R.W., and Burke, D.H. (2007). Active site binding and sequence requirements for inhibition of HIV-1 reverse transcriptase by the RT1 family of single-stranded DNA aptamers. Nucleic Acids Res. *35*, 5039–5050.
20. Michalowski, D., Chitima-Matsiga, R., Held, D.M., and Burke, D.H. (2008). Novel bimodular DNA aptamers with guanosine quadruplexes inhibit phylogenetically diverse HIV-1 reverse transcriptases. Nucleic Acids Res. *36*, 7124–7135.
21. Ditzler, M.A., Bose, D., Shkriabai, N., Marchand, B., Sarafianos, S.G., Kvaratskhelia, M., and Burke, D.H. (2011). Broad-spectrum aptamer inhibitors of HIV reverse transcriptase closely mimic natural substrates. Nucleic Acids Res. *39*, 8237–8247.
22. Whatley, A.S., Ditzler, M.A., Lange, M.J., Biondi, E., Sawyer, A.W., Chang, J.L., Franken, J.D., and Burke, D.H. (2013). Potent inhibition of HIV-1 reverse transcriptase and replication by nonpseudoknot, "UCAA-motif" RNA aptamers. Mol. Ther. Nucleic Acids *2*, e71.
23. Sharp, P.M., and Hahn, B.H. (2011). Origins of HIV and the AIDS pandemic. Cold Spring Harb. Perspect. Med. *1*, a006841.
24. Alam, K.K., Chang, J.L., and Burke, D.H. (2015). FASTAptamer: a bioinformatic toolkit for high-throughput sequence analysis of combinatorial selections. Mol. Ther. Nucleic Acids *4*, e230.
25. Spill, F., Weinstein, Z.B., Irani Shemirani, A., Ho, N., Desai, D., and Zaman, M.H. (2016). Controlling uncertainty in aptamer selection. Proc. Natl. Acad. Sci. U S A *113*, 12076–12081.
26. Darty, K., Denise, A., and Ponty, Y. (2009). VARNA: interactive drawing and editing of the RNA secondary structure. Bioinformatics *25*, 1974–1975.
27. Zuker, M. (2003). Mfold web server for nucleic acid folding and hybridization prediction. Nucleic Acids Res. *31*, 3406–3415.
28. Lange, M.J., and Burke, D.H. (2014). Screening inhibitory potential of anti-HIV RT RNA aptamers. Methods Mol. Biol. *1103*, 11–29.
29. Ozer, A., Pagano, J.M., and Lis, J.T. (2014). New technologies provide quantum changes in the scale, speed, and success of SELEX methods and aptamer characterization. Mol. Ther. Nucleic Acids *3*, e183.
30. Gotrik, M.R., Feagin, T.A., Csordas, A.T., Nakamoto, M.A., and Soh, H.T. (2016). Advancements in aptamer discovery technologies. Acc. Chem. Res. *49*, 1903–1910.
31. Dembowski, S.K., and Bowser, M.T. (2017). Microfluidic methods for aptamer selection and characterization. Analyst (Lond.) *143*, 21–32.
32. Latulippe, D.R., Szeto, K., Ozer, A., Duarte, F.M., Kelly, C.V., Pagano, J.M., White, B.S., Shalloway, D., Lis, J.T., and Craighead, H.G. (2013). Multiplexed microcolumn-based process for efficient selection of RNA aptamers. Anal. Chem. *85*, 3417–3424.
33. Reinholt, S.J., Ozer, A., Lis, J.T., and Craighead, H.G. (2016). Highly multiplexed RNA aptamer selection using a microplate-based microcolumn device. Sci. Rep. *6*, 29771.
34. Wang, J., Gong, Q., Maheshwari, N., Eisenstein, M., Arcila, M.L., Kosik, K.S., and Soh, H.T. (2014). Particle display: a quantitative screening method for generating high-affinity aptamers. Angew. Chem. Int. Ed. Engl. *53*, 4796–4801.
35. Gotrik, M., Sekhon, G., Saurabh, S., Nakamoto, M., Eisenstein, M., and Soh, H.T. (2018). Direct selection of fluorescence-enhancing RNA aptamers. J. Am. Chem. Soc. *140*, 3583–3591.
36. Cho, M., Xiao, Y., Nie, J., Stewart, R., Csordas, A.T., Oh, S.S., Thomson, J.A., and Soh, H.T. (2010). Quantitative selection of DNA aptamers through microfluidic selection and high-throughput sequencing. Proc. Natl. Acad. Sci. U S A *107*, 15373–15378.
37. Berezhnoy, A., Stewart, C.A., Mcnamara, J.O., 2nd, Thiel, W., Giangrande, P., Trinchieri, G., and Gilboa, E. (2012). Isolation and optimization of murine IL-10 receptor blocking oligonucleotide aptamers using high-throughput sequencing. Mol. Ther. *20*, 1242–1250.
38. Thiel, W.H., Bair, T., Peek, A.S., Liu, X., Dassie, J., Stockdale, K.R., et al. (2012). Rapid identification of cell-specific, internalizing RNA aptamers with bioinformatics analyses of a cell-based aptamer selection. PLoS ONE *7*, e43836.

39. Caroli, J., Taccioli, C., De La Fuente, A., Serafini, P., and Bicciato, S. (2016). APTANI: a computational tool to select aptamers through sequence-structure motif analysis of HT-SELEX data. Bioinformatics *32*, 161–164.

40. Hoinka, J., Backofen, R., and Przytycka, T.M. (2018). AptaSUITE: a full-featured bioinformatics framework for the comprehensive analysis of aptamers from HT-SELEX experiments. Mol. Ther. Nucleic Acids *11*, 515–517.

41. Cho, M., Soo Oh, S., Nie, J., Stewart, R., Eisenstein, M., Chambers, J., Marth, J.D., Walker, F., Thomson, J.A., and Soh, H.T. (2013). Quantitative selection and parallel characterization of aptamers. Proc. Natl. Acad. Sci. U S A *110*, 18460–18465.

42. Tome, J.M., Ozer, A., Pagano, J.M., Gheba, D., Schroth, G.P., and Lis, J.T. (2014). Comprehensive analysis of RNA-protein interactions by high-throughput sequencing-RNA affinity profiling. Nat. Methods *11*, 683–688.

43. Buenrostro, J.D., Araya, C.L., Chircus, L.M., Layton, C.J., Chang, H.Y., Snyder, M.P., and Greenleaf, W.J. (2014). Quantitative analysis of RNA-protein interactions on a massively parallel array reveals biophysical and evolutionary landscapes. Nat. Biotechnol. *32*, 562–568.

44. White, R., Rusconi, C., Scardino, E., Wolberg, A., Lawson, J., Hoffman, M., and Sullenger, B. (2001). Generation of species cross-reactive aptamers using "toggle" SELEX. Mol. Ther. *4*, 567–573.

45. Song, M.Y., Nguyen, D., Hong, S.W., and Kim, B.C. (2017). Broadly reactive aptamers targeting bacteria belonging to different genera using a sequential toggle cell-SELEX. Sci. Rep. *7*, 43641.

46. Hamula, C.L.A., Le, X.C., and Li, X.F. (2011). DNA aptamers binding to multiple prevalent M-types of Streptococcus pyogenes. Anal. Chem. *83*, 3640–3647.

47. Shiratori, I., Akitomi, J., Boltz, D.A., Horii, K., Furuichi, M., and Waga, I. (2014). Selection of DNA aptamers that bind to influenza A viruses with high affinity and broad subtype specificity. Biochem. Biophys. Res. Commun. *443*, 37–41.

48. Dupont, D.M., Larsen, N., Jensen, J.K., Andreasen, P.A., and Kjems, J. (2015). Characterisation of aptamer-target interactions by branched selection and high-throughput sequencing of SELEX pools. Nucleic Acids Res. *43*, e139.

49. Madsen, J.B., Dupont, D.M., Andersen, T.B., Nielsen, A.F., Sang, L., Brix, D.M., Jensen, J.K., Broos, T., Hendrickx, M.L., Christensen, A., et al. (2010). RNA aptamers as conformational probes and regulatory agents for plasminogen activator inhibitor-1. Biochemistry *49*, 4103–4115.

50. Michailidis, E., Marchand, B., Kodama, E.N., Singh, K., Matsuoka, M., Kirby, K.A., Ryan, E.M., Sawani, A.M., Nagy, E., Ashida, N., et al. (2009). Mechanism of inhibition of HIV-1 reverse transcriptase by 4′-Ethynyl-2-fluoro-2′-deoxyadenosine triphosphate, a translocation-defective reverse transcriptase inhibitor. J. Biol. Chem. *284*, 35681–35691.

51. Martin, M. (2011). Cutadapt removes adapter sequences from high-throughput sequencing reads. EMBnet.journal *17*, 10–12.

52. Alam, K.K., Tawiah, K.D., Lichte, M.F., Porciani, D., and Burke, D.H. (2017). A fluorescent split aptamer for visualizing RNA-RNA assembly in vivo. ACS Synth. Biol. *6*, 1710–1721.